Cryo-FIB Lift-out and Electron Tomography Workflow for Bacteria-Nanopillar Interface Imaging Under Native Conditions: Investigating Dragonfly Inspired Bactericidal Titanium Surfaces

Chaturanga D. Bandara[1,2,3], Dominik Pinkas[4], Martina Zanova[5], Martin Uher[5], Judith Mantell[2,6], Bo Su[1], Angela H. Nobbs[1], Paul Verkade[2]

1. *Bristol Dental School Research Laboratories, University of Bristol, Dorothy Hodgkin Building, Whitson Street, Bristol BS1 3NY, United Kingdom*
2. *School of Biochemistry, University of Bristol, University Walk, Bristol BS8 1TD, United Kingdom*
3. *Potsdam Imaging and Spectral Analysis Facility (PISA), Helmholtz Centre For Geosciences (GFZ), Telegrafenberg, Potsdam 14473, Germany*
4. *Electron Microscopy Core Facility, Institute of Molecular Genetics ASCR, Videnska 1083, 142 00 Prague 4, Czech Republic*
5. *Tescan Group a.s., Libušina tř. 21, 623 00 Brno, Czech Republic*
6. *Wolfson Bioimaging Facility, University of Bristol, University Walk, Bristol BS8 1TD, United Kingdom*

Abstract

Dragonfly and cicada wing-inspired titanium nanopillar surfaces show promising bactericidal properties for antibacterial medical implant applications, but the precise mechanisms of bacteria-nanopillar interactions under hydrated conditions remain unclear. Cryo-electron tomography (cryo-ET) enables the visualisation of cellular organelles within their native hydrated cellular environment at molecular resolution. Visualising the bacteria-material interface on nanostructured surfaces by cryo transmission electron microscopy (cryo-TEM) requires the preparation of thin lamellae. Obtaining lamellae of bacteria directly on metal substrates while in a non-fixed and hydrated state requires cryo-focused ion beam (cryo-FIB) milling to isolate the targeted bacteria from the bulk sample. This approach faces additional challenges compared to tissues or cells on TEM grids, as titanium samples require a simultaneous cross-section of soft and hard materials at the same position and require vitrification, which embeds the sample in a thick layer of ice. Nonetheless, we demonstrate how to target a specific bacterium interacting with a titanium nanopillar surface using correlative cryo-fluorescence imaging, and how lamellae can still be prepared from vitrified samples by extracting the targeted bacterium and its surrounding as a small volume and transferring it to a receptor grid for thin lamella preparation, called targeted cryo-lift-out. Here, we outline the workflows and discuss their advantages and limitations for producing lamellae through lift-out techniques under cryogenic conditions, using methods that do not involve gas injection systems (GIS) for the lift-out transfer. These advances enhance cryo-ET applications, enabling *in situ* investigations of the interface between bacteria and nanopillars to effectively study the bactericidal mechanisms of biomimetic nature-inspired nanotopographies in a hydrated environment.

Keywords: Cryo-FIB lift-out, bacteria-nanopillar interface, dragonfly wing-inspired, bactericidal, cryo-Electron tomography

Introduction

The rise of antimicrobial resistance (AMR) poses a major global health threat, driving the need for innovative strategies to prevent bacterial infections of medical implants. Biomimetic

nanostructured surfaces with bactericidal properties have emerged as a promising solution in the last decade, particularly those inspired by natural nanopillars on dragonfly and cicada wings.[1-6] Research has shown that bacterial cells that adhere to these biomimetic nanopillar surfaces are non-viable, highlighting a promising alternative to traditional chemical antimicrobials. However, a thorough understanding of the specific bactericidal mechanisms through which these nature-inspired nanostructures eliminate bacteria remains a vital area for further investigation. Advancing this understanding could lead to important insights and developments in antimicrobial strategies for medical implants.

Understanding bacteria-nanopillar interface interactions requires imaging methods that preserve the native hydrated state. While computational models have proposed mechanisms such as membrane stretching, rupture, and cell wall penetration by nanopillars, experimental validation of these hypotheses remains limited under hydrated conditions. Conventional imaging techniques, including scanning electron microscopy (SEM), transmission electron microscopy (TEM), and fluorescence microscopy, have been employed to study these interactions,[5-9] but each comes with distinct limitations. SEM provides a detailed view of bacterial morphology on nanopillar surfaces but cannot capture the critical bacteria-surface interface where interactions occur, whereas this interface can be studied using FIB/SEM. Fluorescence microscopy reveals membrane integrity but lacks the resolution to visualise the nanopillars and damaged bacterial cell wall. TEM offers high-resolution imaging but requires thin, electron-transparent samples, restricting the ability to observe the interactions of an entire bacterial cell with nanopillars. Moreover, traditional electron microscopy techniques require fixation and dehydration, which alter the sample from its native hydrated state and introduce artefacts that can obscure the true bacteria-nanopillar interactions.

To overcome these challenges, correlative cryo-microscopy methods that enable the characterisation of bacteria-nanopillar interactions in their near-native hydrated state and without chemical fixation and dehydration are urgently needed. Cryo-electron tomography (cryoET) facilitates the investigation of ultrastructural studies of bacteria within their near-native state on nanostructured substrates such as titanium medical implants. Gaining insights into the ultrastructure of bacteria-material interfaces in relation to their surroundings is essential for connecting structure with function for biomimetic antibacterial surfaces. Given that the majority of biological specimens are too thick for direct imaging using a cryo transmission electron microscope (cryo-TEM), techniques for reducing biological material thickness to below 200 nm—necessary for electron transparency[10, 11]—have been crucial for making cryoET of internal cell regions and bacteria-surface interfaces possible.

This manuscript presents a cryo-FIB lift-out and cryo-ET workflow to characterise bacteria-nanopillar interactions on dragonfly wing-inspired titanium surfaces, addressing the fixation and dehydration limitations of conventional microscopy approaches used in our previous studies.[5-7, 12] By enabling near-native visualisation of bacteria-biomimetic nanopillar interfaces, while maintaining surface attached bacteria in a hydrated environment this correlative cryo-microscopy pipeline inspires future research that aims to validate computational models and inform the design optimisation of nature-inspired antibacterial surfaces for enhanced efficacy in medical implant applications.

Materials and Methods

Fabrication of nanopillars on titanium by thermal oxidation. Grade V titanium alloy (Ti-6Al-4V) sheets with 75 µm thickness were laser cut into circles of 3 mm or 1.4 mm in diameter. Then

these were hand polished using silicon carbide grit sizes (#2000 and #4000). Then, to remove surface contaminants, titanium disks were placed in an ultrasonic bath (Grant Scientific UXB series), first in acetone followed by distilled water at 40 °C for 15 minutes each using 100% power. Then samples were placed into ethanol (99.9%) for 10 minutes before air drying. Thermal oxidation was conducted as previously reported for titanium nanopillar fabrication.[7, 12] Briefly, titanium samples were sealed inside a horizontal alumina tube (120 cm x 11 cm outer x 9 cm inner) positioned in the tube furnace (Elite Thermal Systems Ltd). Prior to thermal oxidation, the furnace was purged with inert argon gas (Ar) for 30 minutes with 220 sccm to remove oxygen and achieve a one-directional flow. Following the purging, heating started at 10 °C per minute until 850 °C. While maintaining the temperature, Ar was redirected via a sealed bubbler with acetone (99.9%), maintained at 25 °C for 20 minutes. Then the purging via acetone was stopped and Ar was redirected to the tube and cooling was started. This resulted in a black colouration of the samples (Figure 1a). After cooling to room temperature, heating was reinitiated after airing the chamber with ambient air, heated to 600 °C and maintained for 30 minutes for annealing, and then samples were allowed to cool to room temperature overnight. This served to remove the C from the samples (Figure 1b). These samples served as the substrates for this experiment.

Culture of bacteria. *Escherichia coli* strain K12 was used as a model bacterium in this study. Luria Bertani broth cultures were incubated for 16 h at 37 °C, 200 rpm, then subcultured to OD_{600} 0.1 and grown to mid-exponential phase before use in the experiment. For incubation on titanium substrates, cultures were diluted to OD_{600} 0.1 in Luria Bertani broth. Titanium samples were sterilised in 70% ethanol, washed in dH_2O, dried and stored until the experiment. Immediately prior to inoculation, titanium substrates were glow-discharged using Leica EM ACE600 (Leica Microsystems) to become hydrophilic. Without this step, inoculation was challenging, as the titanium sample bound to the end of the pipette tip when liquid transfer.

Cryo vitrification. Cryo-lift-out starts with the cryo vitrification step to achieve a vitreous ice sample. We have tested both plunge freezing (PF) and high pressure freezing (HPF) in this experiment, as illustrated in Figure 1.

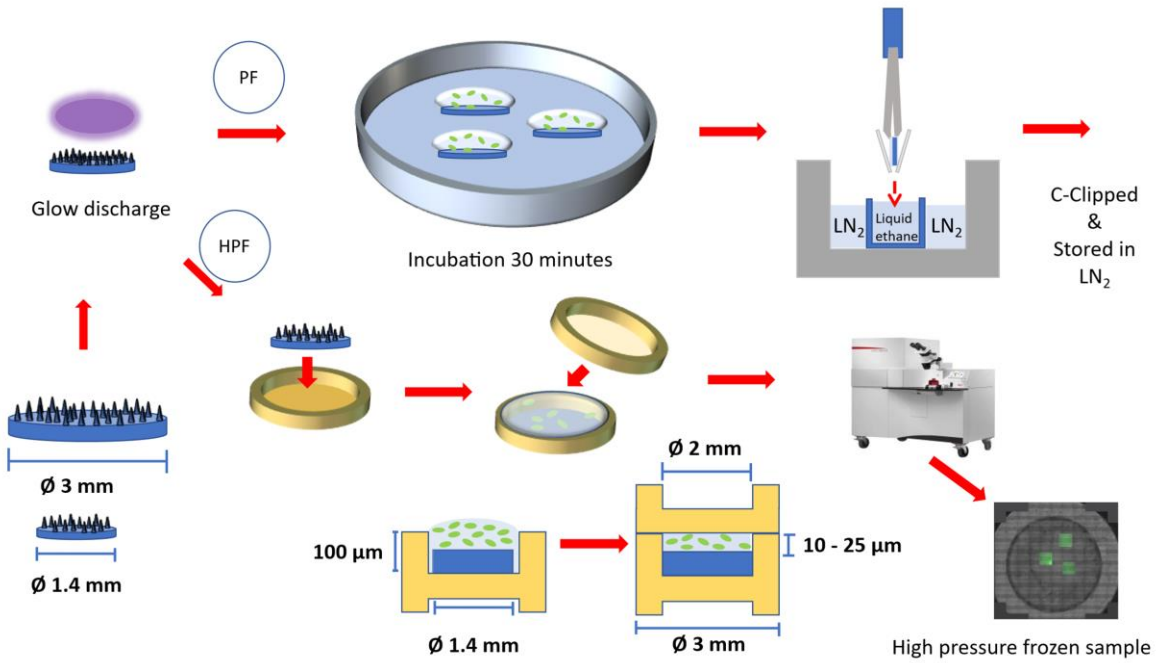

Figure 1: Illustration of cryo vitrification of samples. PF: Plunge freezing, HPF: High pressure freezing.

For plunge freezing, cells were vitrified using a Leica EM GP2 (Leica Microsystems). A 20 µL aliquot of bacterial suspension was applied to the sample and incubated for 20 minutes at room temperature. Then, 10 µL of SYTO9 was added to stain the bacterial cells. After 10 minutes, these samples were transferred to a Leica EM GP2 plunge freezer at humidity 80%, samples were blotted for 4 seconds with filter paper and immediately frozen in liquid ethane/propane mixture maintained at liquid nitrogen temperature. Samples were then clipped into a TEM AutoGrid (Nanosoft) cartridge with the cell side facing down and stored in liquid nitrogen until imaging.

High-pressure freezing

High-pressure freezing was performed using a Leica EM ICE system. Samples at room temperature were added with 50 µL of *E. coli* suspension for 20 minutes in 3 mm copper planchets. Syto9 (50 µL) was then added for a further 10 minutes to stain the bacterial cells. These titanium samples with surface-attached bacteria were topped with a marked cap wetted with 1-hexadecene to facilitate detachment. Samples were rapidly vitrified under a pressure of 2100 bar and cooled to −196 °C within milliseconds in the Leica EM ICE high pressure freezer. Following freezing, samples were stored in liquid nitrogen until further processing. The resulting vitrified layer was approximately 25 µm thick, fully embedding the bacterial cells and preserving their hydrated state. The vitrified HPF carriers were manually opened within the cryo-CLEM loading station (Leica Microsystems, Vienna, Austria) immersed in liquid nitrogen. This was achieved by carefully pushing the planchets apart using tweezers. Once opened, the bottom carrier containing the sample was loaded into a custom-designed cartridge for transfer into the microscopes.

Cryo-Sample Handling and Transfers between different modalities

Maintaining vitrified samples in a stable cryogenic and contamination-free state throughout the correlative cryo-microscopy workflow is essential for preserving ultrastructure and enabling accurate multi-modal imaging of bacteria-nanopillar interfaces. A major logistical challenge in this workflow was the safe and efficient transfer of frozen-hydrated samples between multiple instruments, including the cryo-fluorescence microscope, cryo-coating system, cryo-FIB/SEM, and cryo-TEM, while preventing devitrification and minimising ice contamination.

To address this, all sample handling and transfers were conducted using the Leica EM VCM system and Leica EM VCT500 shuttle. The Leica EM VCM provided a temperature-controlled cryo-loading interface, maintained at liquid nitrogen temperature, allowing sample manipulation and orientation in a protective nitrogen atmosphere without devitrification or minimal frost contamination to exchange samples between the cryo-fluorescence microscope and cryo-FIB/SEM. This interface enabled transitions with specific sample holders required between devices while preserving sample integrity. This integrated handling approach was essential for bridging different modalities and enabling accurate correlative imaging. The Leica EM VCT500 served as a vacuum cryo-shuttle, enabling contamination-free transfer of samples to the Leica cryo-coater and Tescan cryo-FIB/SEMs.

Overview of Cryogenic Imaging Workflow

To preserve the native ultrastructure and spatial context of bacteria at the nanopillar interface, imaging was performed under fully hydrated conditions using cryo-FIB/SEM, cryo-fluorescence

and cryo-TEM. This approach enabled high-resolution visualisation of bacterial cells on biomimetic nanostructured surfaces without chemical fixation, dehydration, or heavy metal staining, as required for conventional EM preparation. To maintain *in situ* positioning, bacteria were vitrified directly on titanium test samples, ensuring that cells remained undisturbed at their original locations. The cryogenic workflow preserves the physiological integrity of both the cells and the surrounding material, allowing accurate correlation between morphology and function in a near-native hydrated environment at the time of imaging.

Achieving effective vitrification directly on test substrates was a critical challenge. Both plunge freezing and HPF methods were explored in the experiments. Plunge freezing yielded a vitrified layer ~5 µm thick, while HPF resulted in a thicker layer of ~25 µm. As bacterial cells (~1 µm in diameter) interacting with the surface were entirely embedded within the vitrified volume, they were not visible by SEM alone, complicating direct targeting of bacteria for cryo-ET.

To address this, correlative cryo-fluorescence microscopy was employed to localise regions of interest prior to FIB milling. However, the absence of fiducial features that were simultaneously visible in both fluorescence and electron modalities limited the precision of image registration. This was mitigated by two approaches; 1) by adapting to surface cracks or 2) making fiducial marks on the vitrified sample surface using FIB/SEM. A final constraint was the requirement for electron-transparent lamellae for cryo-TEM. To achieve this, selected regions identified by cryo-fluorescence were isolated and extracted onto a TEM grid using FIB/SEM with a cryo-cooled nanomanipulator and finally thinned to <200 nm, enabling high-resolution structural analysis of the bacteria-nanopillar interface by cryo-TEM.

In the following sections, different methods and challenges faced and how they were mitigated are extensively discussed.

Cryo light microscopy (cryo-LM)

The carrier containing the sample was loaded into a custom-designed cartridge for transfer into the Leica EM Cryo CLEM Thunder Imager system (Leica Microsystems, Austria). The sample was maintained in overpressure of cold nitrogen gas to maintain a vitrified state and avoid contamination with atmospheric humidity. Images were acquired with 50x dry objective with NA of 0.9 (HC PL APO, CRYO CLEM, Leica Microsystems) equipped with a Leica DFC9000 GT camera. Light microscopy images were captured in reflected light and fluorescence (EX 450-490nm, EM 500-550nm) modes. Large areas were imaged via stitching of multiple individual exposures using the Leica Navigator module within LAS-X software package. Images were captured at a frame size of 2048 x 2048 pixels, resulting in a pixel size of 0.13 µm. Manufacturer recommended system-optimized Z-steps were of 0.44 µm were used. The exposure time of 100 ms in channel 1 (SYTO9, green fluorescence) and 1 ms in channel 2 (REF, reflection, grey). To improve the clarity of the fluorescence datasets and enable reliable correlation with the cryo-FIB-SEM step, the Z-stacks were processed using the proprietary GPU accelerated Leica Thunder deconvolution technique in the LAS X software (Leica Microsystems, Vienna, Austria). The marked fiducials and fluorescence data were combined in Fiji, and the resulting composite images were exported in TIFF format and subsequently used as reference maps for cross-modality alignment (Figure 4a).

Cryo-correlation of fluorescence data and ion beam field of view for selecting a single-bacterium for lift-out

Since bacteria were hidden below the surface, and surface topography of vitrified samples did not indicate the presence of bacteria, cryo-fluorescence and cryo-FIB/SEM data were required to produce a targeted cryo-lamellae from vitrified samples. Moreover, fluorescence and topographical surface features were not available simultaneously from the same feature in the two independent systems. Thus, a complex workflow was required to accurately extract a targeted bacterium for cryo-tomography data acquisition. We tested two different approaches: first, using dominant surface features, then second, using marked fiducials via the Ga-FIB on the surface, as illustrated in Figure 2.

Correlative Registration Protocol based on surface features. A clearly recognisable feature on the sample surface was recognised using the fluorescence microscope. In this instance, the 10x10 µm FIB milled area with surface cracks were picked. Then a reflectance light imaging and a fluorescence imaging of the same area was acquired and fluorescence and reflected light channels were merged into a composite image. Surface features, including cracks, and ice forms were visible in the composite image, along with fluorescently labelled bacteria. Then the sample was transferred to Ga-FIB under cryo conditions, and the same field of view was relocated. Excessive ice formations were milled away by scanning with the ion beam at a lower magnification to facilitate recognition of the surface features. Then the reflected light image was overlayed using Tescan Coral software by selecting correlated positions (C1, C2, and C3) in both FIB and imported reflected light image. Then acquired Z-stack was analysed to identify bacterial cells located at the bottom of the fluorescence volume (i.e., adjacent to the titanium nanopillar surface). Only positions of these surface-associated cells were selected for lamella preparation to enable investigation of bacteria-material interactions via cryo-ET.

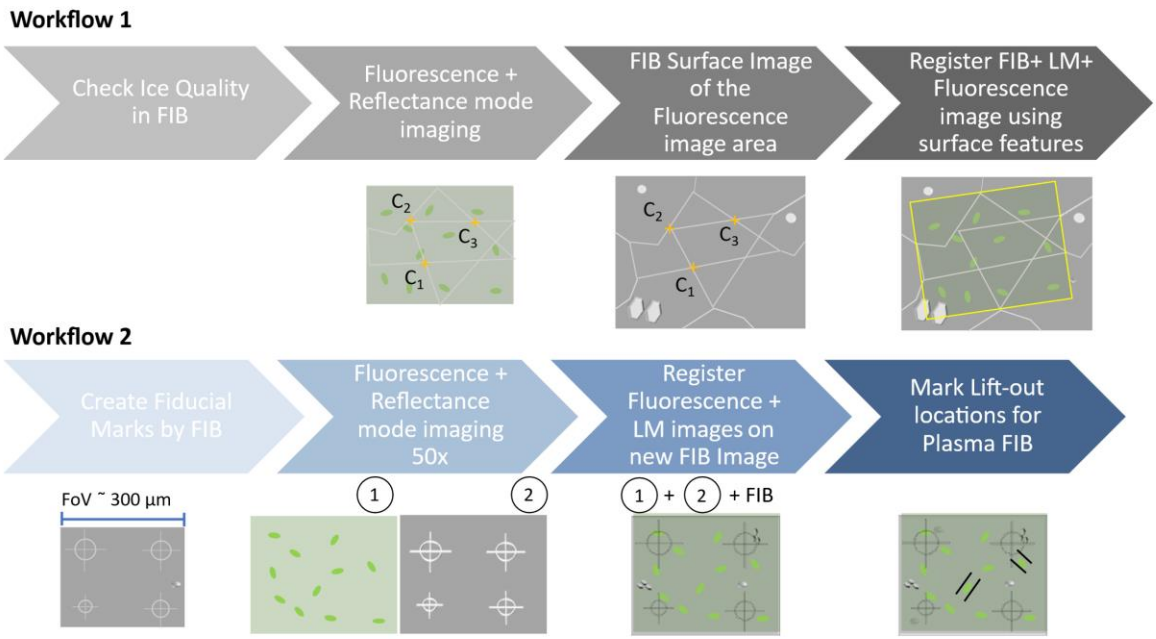

Figure 2: Two different correlative microscopy approaches used in this work. Workflow 1: With Tescan Essence software with surface cracks. Workflow 2 With defined fiducials on the surface of the sample using Ga-ion beam. Marked fiducials are visible in the 50x field of view in the reflectance mode. Their asymmetry helps to identify the sample when the fluorescence microscope provides flipped images. Finally the lift-out locations are marked by two lines centring a single bacterium.

Fiducial Marker Fabrication and Correlative Registration Protocol

Fiducial marker creation. Three discrete regions on the vitrified sample were randomly selected and marked using the Ga-FIB Cryo-SEM system. In each region, four fiducial patterns comprising crosses and circles of different sizes were milled in a square configuration to form a recognisable layout (Figure 2) visible under the cryo-fluorescence microscope with 50x objective, and fitting all fiducials within a single field of view of 300 µm.

Cryo-fluorescence imaging and target selection. In the cryo-fluorescence microscope, fiducial patterns were first identified using the reflected light channel. Each region of interest was centred within the square formed by the four fiducials. Single reflectance mode image and fluorescence Z-stacks were acquired to image bacteria within the marked field. Then maximum intensity projections were generated, and fluorescence and reflected light channels were merged into a composite image. Z-stacks were analysed to identify bacterial cells located at the bottom of the fluorescence volume (i.e., adjacent to the titanium nanopillar surface). Only positions of these surface associated cells were selected for lamella preparation to enable investigation of bacteria-material interactions.

Correlative registration in cryo-FIB/SEM. Subsequently, the samples were transferred to the cryo-FIB/SEM for the second time, and the marked fiducials were located. Then the composite fluorescence data were imported into the Tescan CORAL module embedded within the Tescan ESSENCE software package used to control the FIB-SEM instrument. The fluorescence images were registered to the ion beam field of view using fiducial markers as anchor points. Based on Z-stack data, precise lift-out locations were defined and targeted for lamella preparation. Identified lamella locations consisted of two 10 µm × 2 µm rectangles straddling a bacterium. To mitigate the risk of fiducials being obscured by ice contamination during storage or transfer, several marked areas were generated as backups. Then Multi-scale "Zoom-in" maps (Supporting Information) of each fiducial-marked region were created in Ga-FIB/SEM to guide the plasma FIB/SEM operator in efficiently navigating to regions of interest and executing high-precision lift-outs. Samples were stored in liquid nitrogen, and transported to the next site in a dry shipper until plasma-FIB/SEM preparation.

Correlation of a light microscopy volume image and EM field of view presents inherent challenges due to the significant differences in resolution and field of view between the two modalities. Cryo-sample preparation and cryo-plasma FIB/SEM imaging were conducted at two separate facilities. As the plasma FIB/SEM system lacked an integrated cryo-fluorescence microscope, it was essential to predefine and mark regions of interest for lamellas in advance. Mapping the entire sample at nanometer precision is impractical and prone to error due to the image stitching process, ice contamination, and the inherent complexity of spatial correlation. To overcome this challenge, we developed a novel fiducial marker strategy to enable reliable localisation of bacterial targets with high spatial precision.

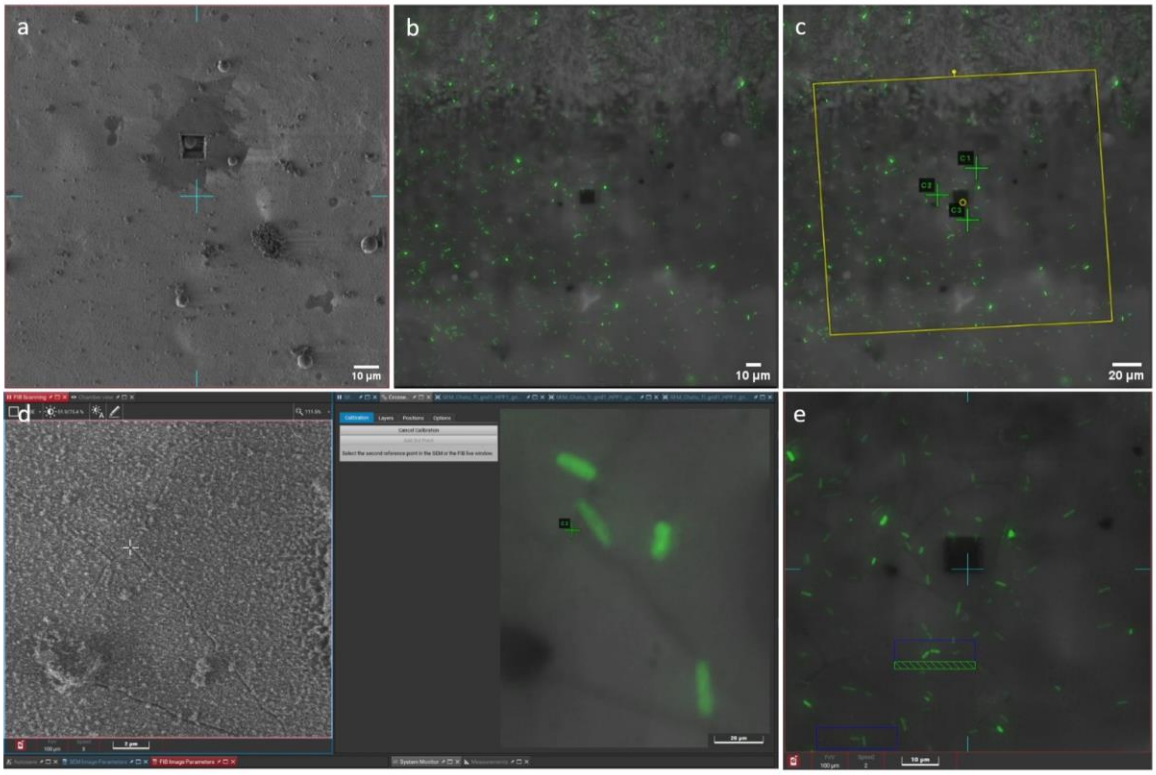

Figure 3: Correlation of fluorescence data with FIB SEM image using Tescan Essance software. a) FIB/SEM image showing the area where ice quality was checked. The prominent square is clearly visible in both FIB/SEM and in brightfield mode. b) 50X map of bacteria and overlay with brightfield images. c). Successful overlay of fluorescence data with FIB view. d) Tescan Essence software interface picking the second point in fluorescence image (right) and on FIB view (left) during image correlation. The cross in the centre of FIB view corresponds to position C_2. e) Selection of two bacterial cells of interest in the FIB (marked in blue). Screen views are adjusted for brightness and contrast for clear visualisation.

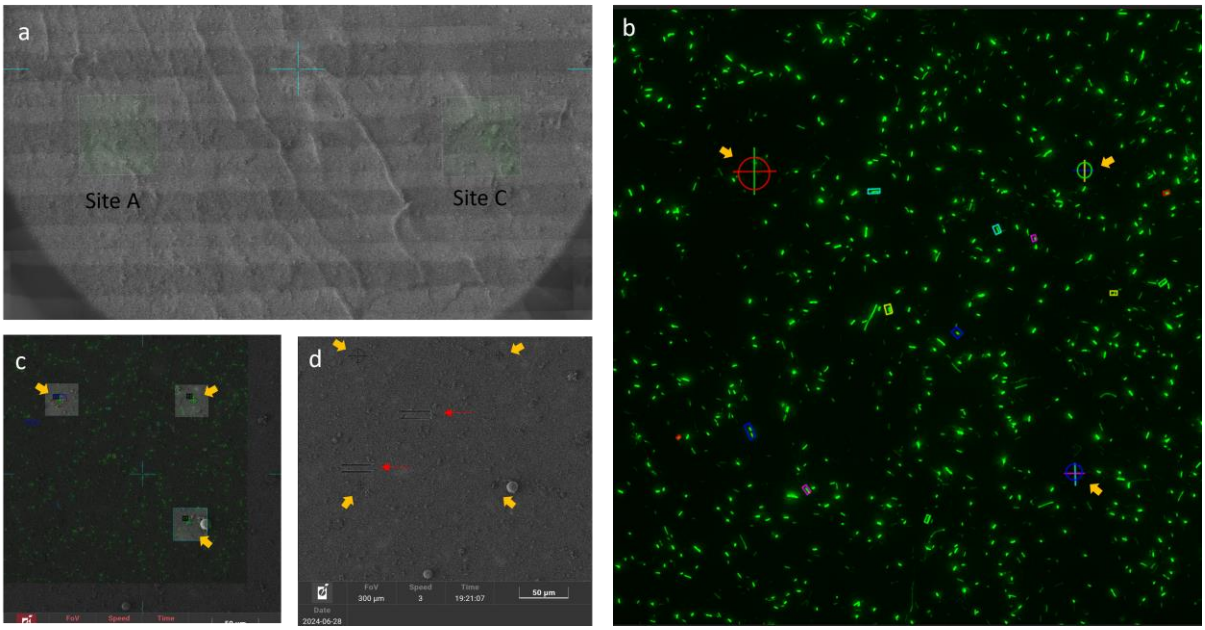

Figure 4: Fiducial marker-based identification of ROI's with bacteria for lift-out preparation. a) Overview of larger area of sample with multiple areas marked with fiducials (green colour area). Fiducials are not visible, but approximate locations of sites are identifiable. b) Fluorescence image of a single site shows bacteria in green and the fiducials visible (yellow aroows) in reflectance mode is marked to a single image. Bacterial cells at the bottom of the Z stack are identified as regions of interest for FIB liftouts. c) fluorescence data is registered to FIB image, and d) Two liftout

positions per area are marked (red arrows) to perform liftout without the need of fluorescence microscope in the other facility.

Cryo FIB/SEM Lift-out preparation

Cryo-FIB-SEM experiments were conducted on Tescan AMBER Ga FIB/SEM and Tescan AMBER X2 Xe plasma FIB-SEM systems (Tescan) equipped with a Leica VCT500 cryo stages. In the Leica VCM loading station (Leica Micro-systems), HPF samples were mounted on a 30° pre-tilted prototype Leica cryo holder compatible with HPF carriers and Autogrids for lamella preparation. Using the Leica VCT500 Shuttle, the mounted sample holder was transferred into the Leica ACE600 cryo-sputter coater (Leica Microsystems) at a cryo-stage temperature of -150 °C and samples were sputter-coated with a 10 nm thick Pt layer. The samples were transferred to the Tescan FIB/SEM using the VCT500 Shuttle and a layer of platinum pre-cursor was deposited onto the sample surface to minimize the curtaining effect using gas injection system (GIS).[13] The stage temperature was maintained below -150 °C and the system vacuum below 1.4 x10^{-6} mbar pressure. Due to the complexity and material properties of the titanium substrates used, a hybrid FIB strategy combining Ga-FIB and plasma FIB was adopted to optimize both milling efficiency and lamella quality.

1. *FIB/SEM - Ga:*

Vitrified samples were transferred under cryogenic temperatures into the Tescan AMBER Cryo Ga FIB/SEM (Tescan, Czech Republic) using a precooled cryo stage maintained below –150 °C. The preparation workflow consisted of four main steps: trench milling, rough polishing, lamella extraction and final thinning.

Once the location of the bacterial cell was identified, three trenches were made around the target lamella area using the Ga ion beam, resulting in a block of material. Initially, stepwise cutting was performed with a depth of 30 µm. Then the redepositions were cleaned multiple times around the block of material and a cleaning cross sections were performed to make sure the desired level of depth was achieved. All sides were polished with a moderate current (30kV, 20nA) to make sure the target lamella was separated from the bulk material from three sides. The sample was then rotated 180° and the lamella was cut from the underside to separate it from the bulk material underneath yet still attached on one side. At this stage, the sample was stored overnight and on the next day, any ice contaminations were cleared by scanning with the ion beam at low magnification. After rotating the sample back to the initial milling direction, all sides were checked to ensure that the milled pillar was completely separated on three sides and the bottom, enabling the sample to proceed to the lift-out transfer step.

2. *FIB/SEM – Plasma:*

It was evident that Ga FIB was not efficient for extracting a titanium slab from bulk material, hence cryo Plasma FIB/SEM was adapted for lift-out preparation. Once vitrified, samples with marked lift-out locations were transferred under cryogenic temperatures into the dual-beam cryo-plasma FIB/SEM Tescan AMBER X2 (Tescan, Czech Republic) using a precooled cryo stage maintained below - 150 °C. The preparation workflow consisted of four main steps: trench milling, rough polishing, lamella extraction and final thinning.

Trench milling and lamella in-trench polishing using Xe Plasma FIB

Initially, pre-marked fiducials were identified in the SEM under low magnification. A Pt layer was deposited using an ion beam assisted gas injection system to cover and protect the region of

interest from ion damage during the milling process. Using a xenon plasma ion beam at high current (30 kV, 60 nA), three trenches were milled around the target lamella area, resulting in a thickness of 10 µm x 30 µm containing the pre-identified bacterium. Then all slides were polished with a moderate current (30 kV, 20 nA) to reach a suitable lamella size for cryo lift-out. The sample was then rotated 180° and all the lamellae were undercut to make sure that the ROI was fully separated from the bulk sample on the bottom side and yet hanging only from one end. One lamella was lifted out of the trench using Xe Plasma FIB. The two other lamellae were transferred under cryo conditions back into storage until the lift-out and polishing steps.

Lift-out transfer

In Ga-FIB/SEM, pre-milled areas were found under low magnification. The ice contamination from the transfer was removed using the Ga ions. A Tescan cryo-nanomanipulator (Tescan, Czech Republic) was used to lift out the lamellae from the bulk sample. The nanomanipulator was brought closer and attached to the lamella using redeposition while making 4 cuts of 200 nm size on the sample (30 kV, 3 nA). Then the side connection was cut off (30 kV, 3 nA) with an ion beam and the cryo lamella was carefully lifted out, brought closer to the FIB liftout TEM grid. Transferred by using redeposition by making 4 cuts as before on the samples and TEM grid (30 kV, 1 nA). Then the lift out was released from the nanomanipulator by sectionning the initial redeposition (30 kV, 1 nA). These lamellae were thinned from both sides using a stepwise reduction in ion current from 3 nA to 50 pA, until a final thickness suitable for cryoET of approximately 200 nm was achieved.

Cryo TEM

Thin lamellae were transferred into cryo TEM (Jeol JEM-F200, Jeol, Japan) in a LN2 cooled Simple Origin Model 210 tomography cryo transfer holder (Simple origin, PA, USA). Samples were observed using a 200 kV Jeol TEM (Jeol, Japan) microscope with TVIPS TemCam XF-416 CMOS based camera (TVIPS, Germany). Tilt-series were acquired using the SerialEM software package from -60° to +60° tilt with 3° increment[14], utilizing a dose symmetric acquisition scheme.[14, 15]

Results

Generation of nanopillars on titanium by thermal oxidation

The thermal oxidation method generated the nanopillar samples used for the study (Figure1). After initial exposure to acetone, the sample appeared black in colour (Figure 1a) and after oxidation, samples appeared a in yellow/blue colour (Figure 1b). Overall, the samples appeared flat (Figure 1c), but their surface comprised highly dense nanopillars (Figure 1d) and from the side view (Figure 1e), they were not flat.

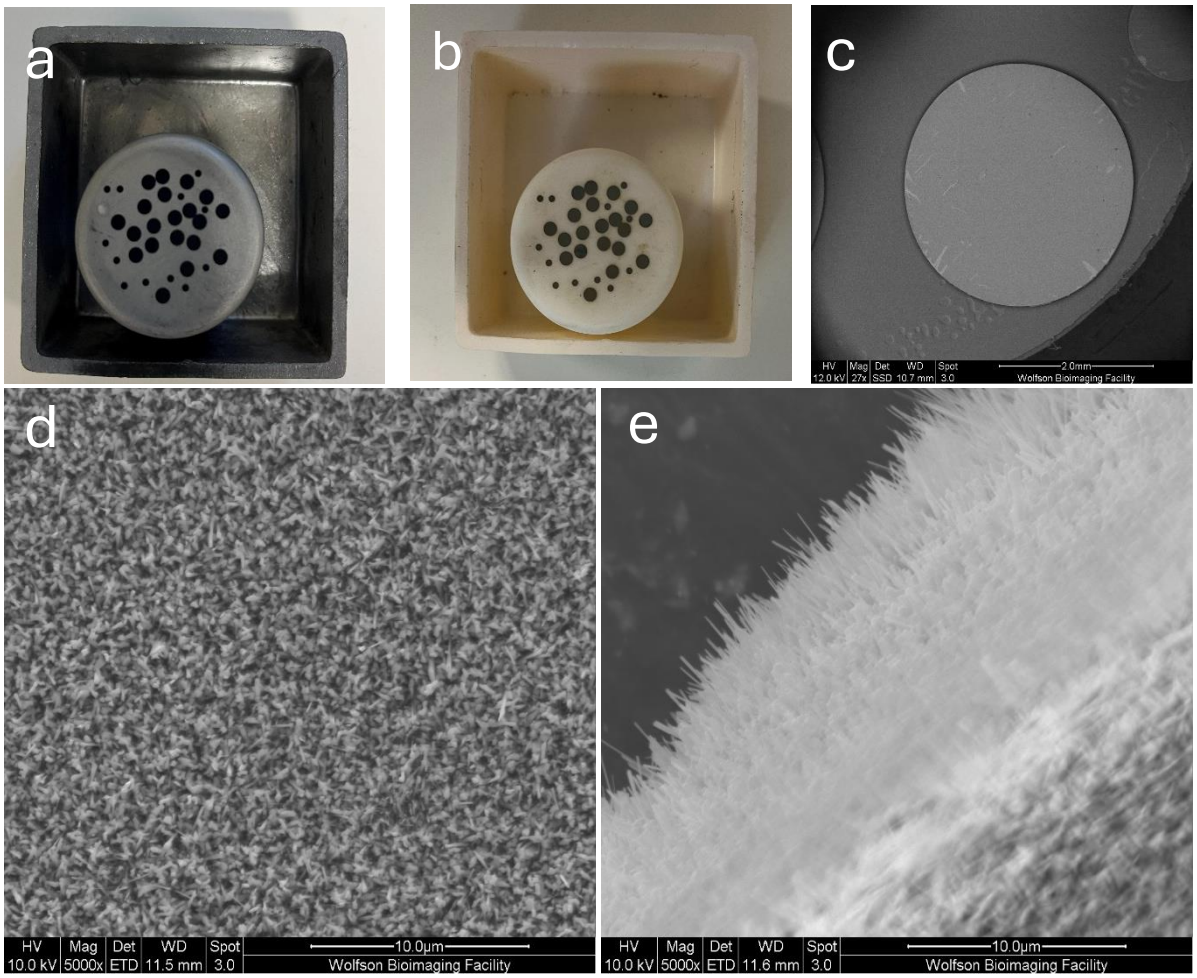

Figure 5: Fabricated nanopillar titanium sample. a) Samples after treated with acetone; b) Samples after oxidation in air; c) SEM micrograph showing the appearance of the nanopillar fabricated sample; d) SEM micrograph showing the top view of the fabricated surface with densely packed nanopillars; e) SEM micrograph showing a tilted view where protruding nanopillars are visible.

Isolation of single bacterium and TEM lamella preparation (Figure 6&7)

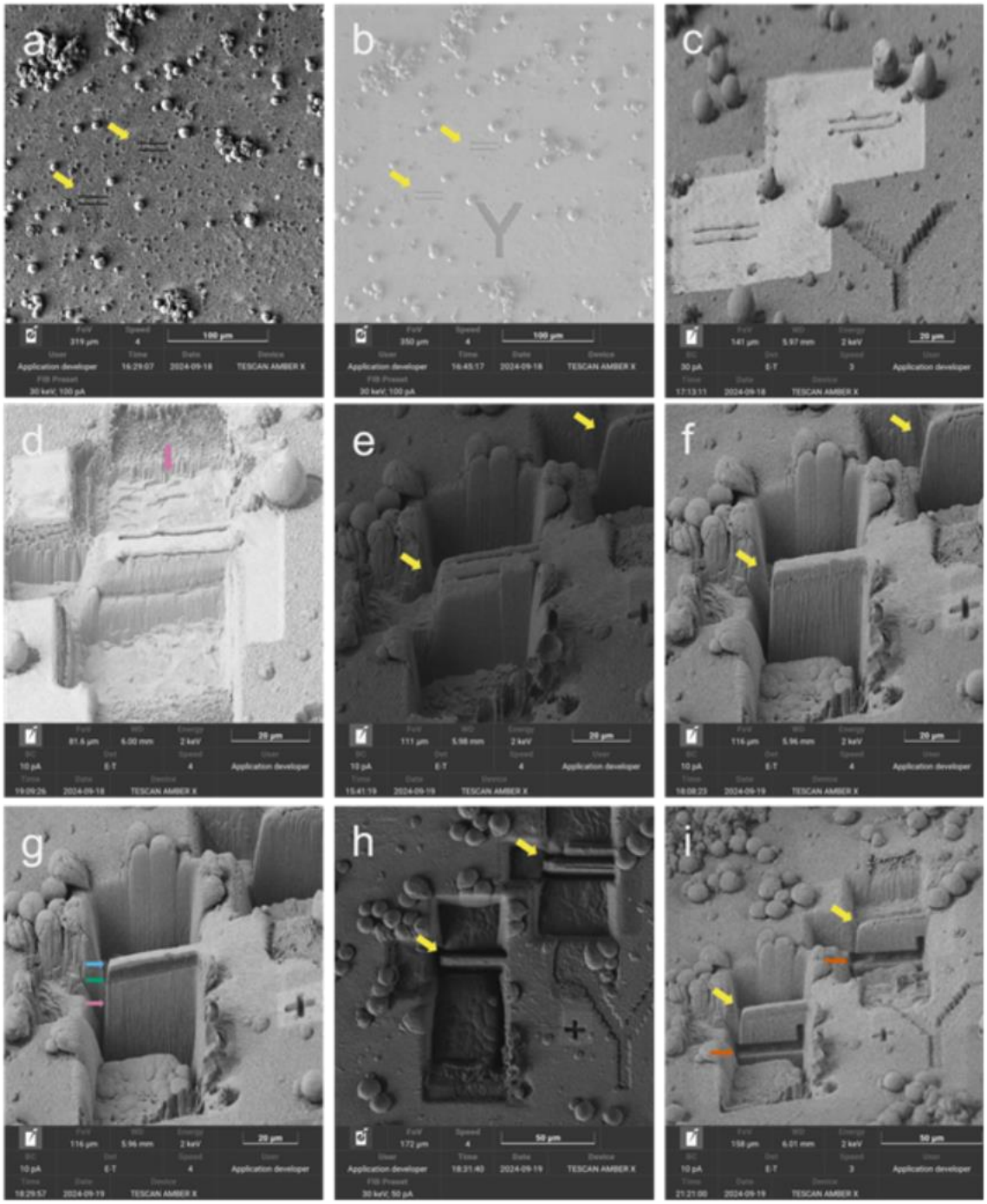

Figure 6: Isolation of a single bacterium for TEM tomography by targeted cryo-liftout using FIB/SEM. a) The two yellow arrows point to two positions where two lamellae were to be prepared for cryo tomography. b) Letters A and Y was used to mark the areas before depositing a protective Pt layer. c) Area after Pt deposition, in preparation for milling. d) Trenches around one lamella being cut. Pink arrow indicates the exposed titanium. e) Trenches are cut to expose the areas of two lamellae. f) Deep trenches are cut, with the lamellae shown before polishing. g) One lamella is polished to show the different layers. Blue arrow, protective Pt layer; green arrow; vitrified water layer with bacteria; pink, titanium surface. h) Top view of the area in a) after trenches are cleared before the undercut. i) Undercut (orange arrow) has been performed, with the lamella now hanging to the titanium base from the side

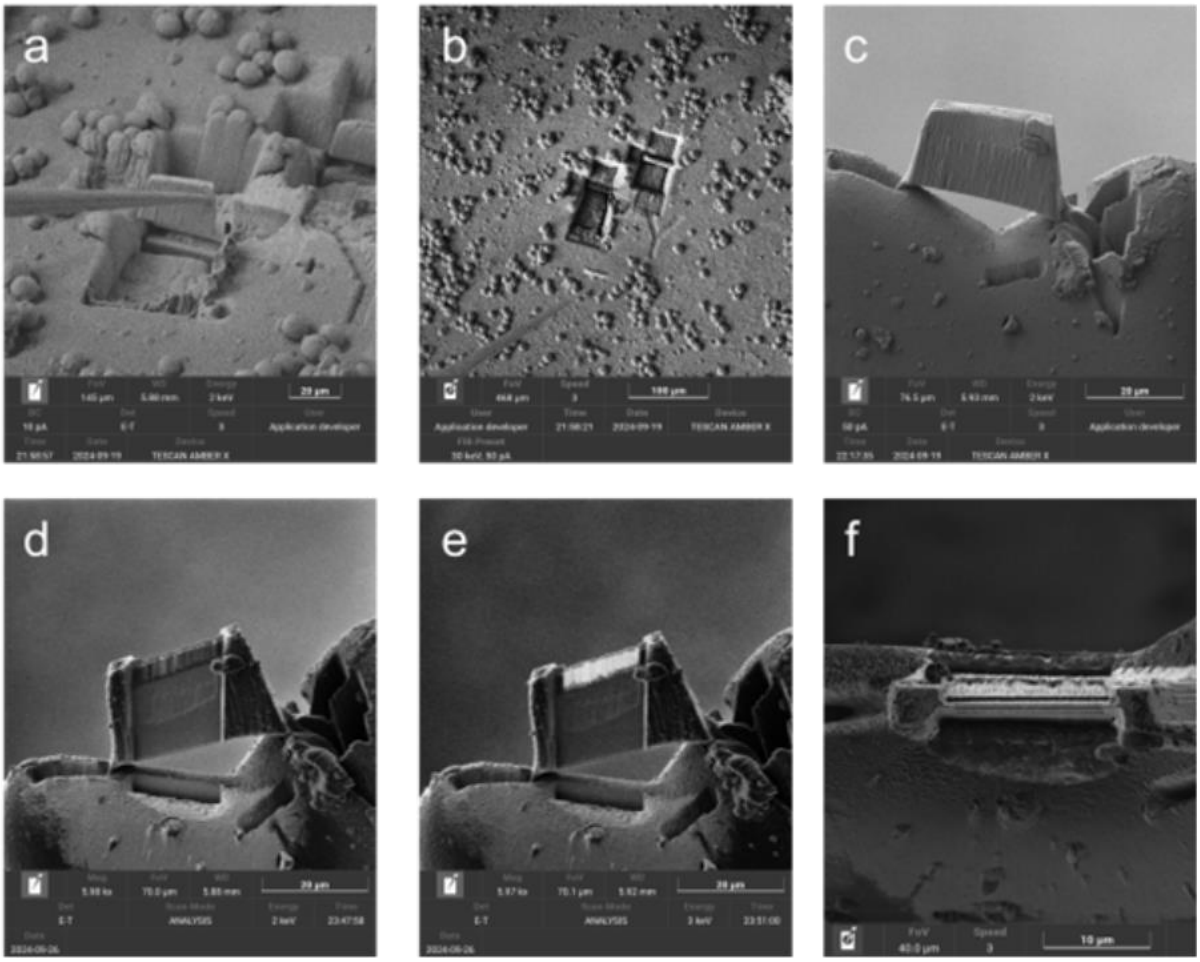

Figure 7: Lift-out of the lamella to electron transparent sample prepared in vitrified sample. a) A lamella lift-out using a cryo needle. b) Overview image of the lamella being removed from the original site c) attached lamella, and d-e) progressive steps of lamella polishing f) Top view after polishing of the lamella.

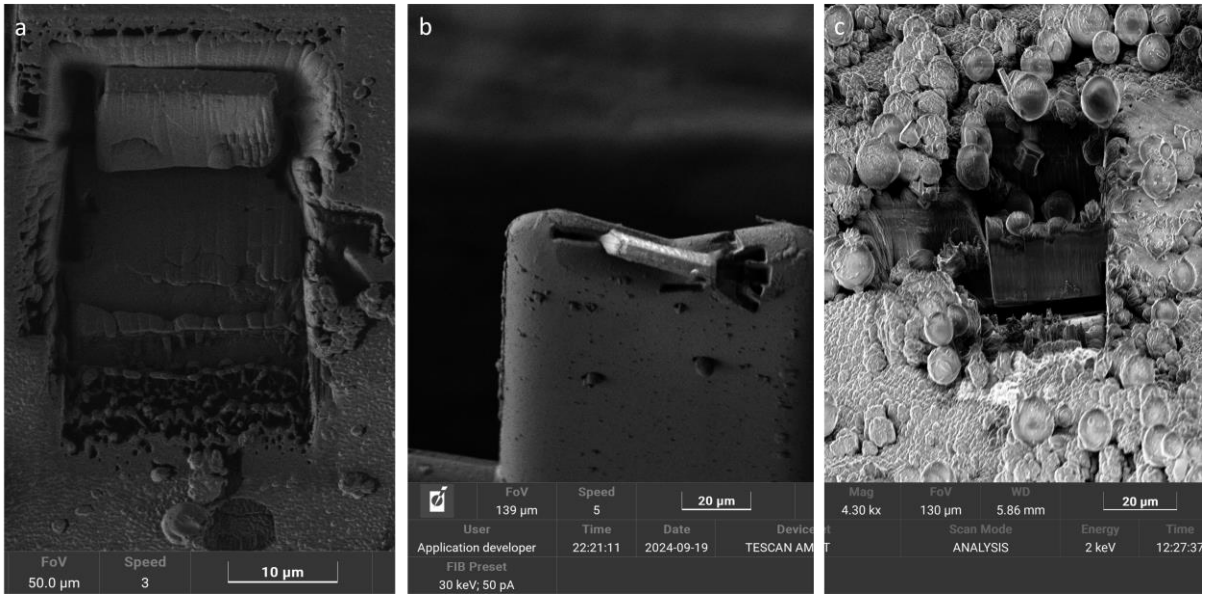

Figure 8: Challenges in the Workflow. a) A lift-out was attached at the bottom during Ga-FIB/SEM preparation, hence it could not be lifted out easily. b) Lamella lift-out by Plasma FIB/SEM but failed upon transfer to the TEM grid. c) Ice contamination of the sample after storage and lamella is partially covered by ice.

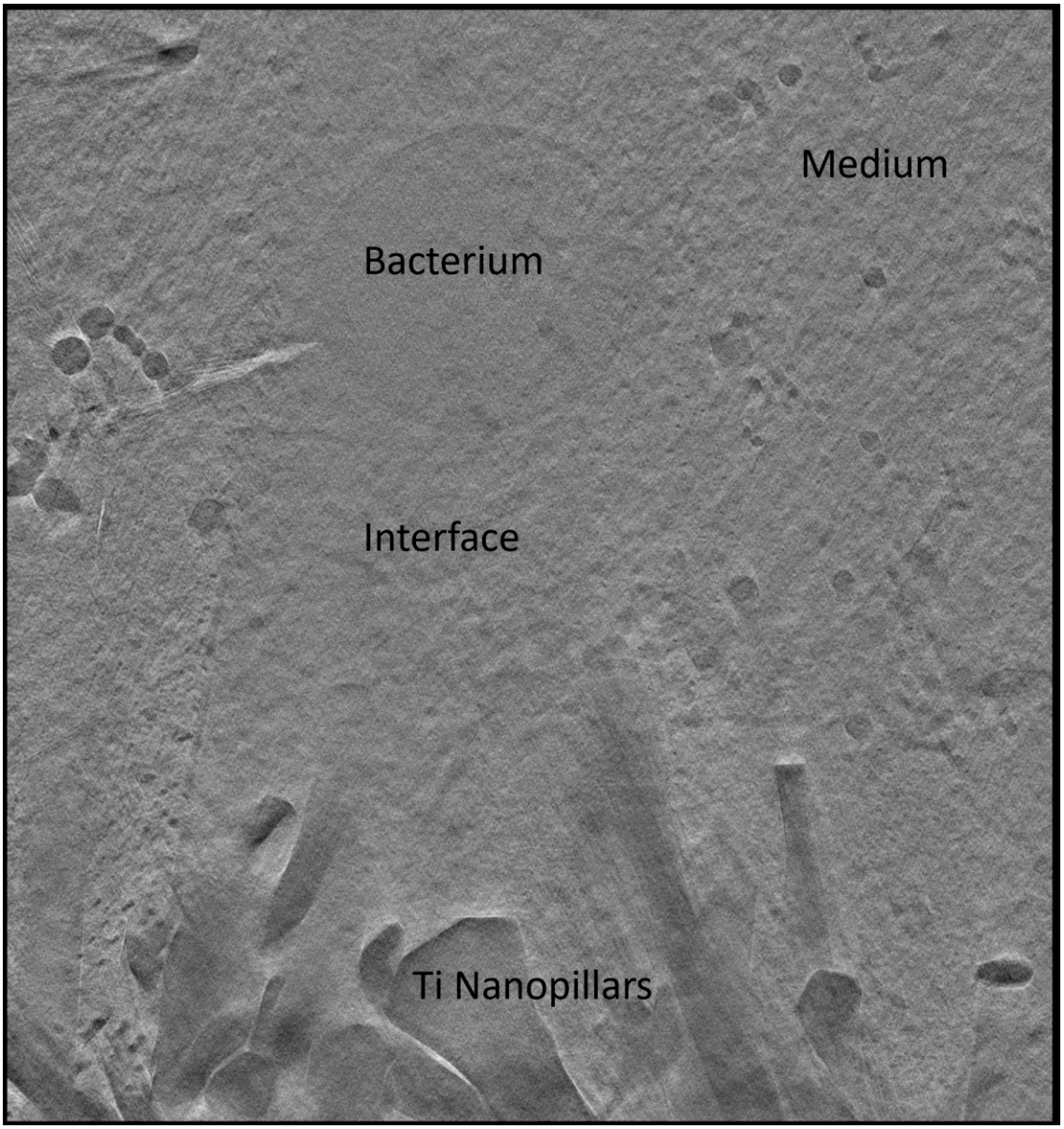

Figure 9: Cryo TEM Tomogram showing nanopillar-bacteria interface in near-native hydrated state

The main aim of this study was to establish a workflow to characterise the bacteria-nanopillar interface under hydrated conditions. Here we show the bacteria-titanium interface under hydrated conditions, where no chemical fixation, dehydration or resin embedding was used in the workflow. The nanopillars and the bacterial cell-wall are clearly visible, and the interface is filled with the media and no air bubbles. We have targeted a bacterium attached to the surface, but we can see a 100-200 nm gap between the top of the nanopillars and the bacterial cell wall. During initial screening using fluorescence microscopy, we were unable to visualise the nanopillars and so it was not possible to ascertain definitively where nanopillars made direct contact with bacterial cells. Nevertheless, this image provides a proof-of-principle that bacteria-nanomaterial interfaces can be studied with cryo-microscopy approaches.

Discussion

Overview of workflow performance

This study successfully established a correlative cryo-electron tomography workflow for targeting a specific bacterium interacting with a nanopillar surface on clinically relevant titanium substrate under near-native hydrated conditions. Despite the challenges of working with non-standard cryo-EM substrates and across geographically separated cryo-microscopy facilities, we demonstrate that high-resolution structural analysis of bacteria-material interactions is achievable with appropriate methodological adaptations.
Key achievements include: Substrate optimisation, Fiducial-based correlation, Hybrid FIB strategy and Proof-of-concept tomograms, validating the complete workflow from vitrification through to tomographic reconstruction.

Workflow reproducibility and scalability

The described workflow is fully reproducible using commercially available cryo-infrastructure and can be adapted to a range of bacterial strains and surface topographies. While HPF is preferred for optimal sample thickness and hydration, the workflow is also compatible with plunge freezing for thinner specimens. However, this depends on the thermal properties of the substrate used. The modularity of the workflow, including cryo-compatible shuttles, transfer stations, and correlation strategies, allows for integration into existing cryo-electron microscopy pipelines. Compared to conventional room-temperature preparation[1] or cryo-ET on grid-adhered cells, this substrate-based *in-situ* workflow enables characterisation of cell–surface interactions under fully hydrated conditions, without need of further manipulation of cells (e.g. removal of cells or nanopillars from the original contact point) or of chemical fixation, which alters the bacterial cell wall. This approach therefore offers a scalable and transferable method for investigating bacteria-material interfaces in a hydrated state with nanoscale resolution and to study the fate of the bacterial cell wall upon interacting with bactericidal nanopillar topographies.

Success metrics and limitations:

While the workflow proved technically feasible, **reproducibility remained sample and operator-dependent**, with notable challenges in milling efficiency, lift-out reliability and precision of correlation. Ice contamination during multi-facility transport and electrostatic issues during lamella transfer represented significant bottlenecks affecting overall yield. Every remount and transfer step can introduce ice contamination or total loss of the sample while manual handling. These limitations underscore the conclusion that while the approach is scientifically valid, further instrumental and procedural refinements are needed to achieve routine, high-throughput applications.

The following sections discuss the strategic decisions, technical considerations, and future directions that emerged from this work, paving the way for exciting new developments in the field.

Substrate Design and Preparation Strategy for Correlative Cryo-Imaging

The choice of substrate material for developing this workflow involves a critical trade-off between cryo-vitrification efficiency and clinical translatability. In the cryo-EM field, sapphire disks have emerged as the gold standard for high-pressure freezing due to their exceptional thermal conductivity (23-40 W/m.K), enabling rapid heat extraction and consistent vitrification of biological samples.[16-18] However, sapphire is not a material used in load-bearing medical implants due to its limited fracture toughness. Moreover, creating biomimetic nanopillar arrays on sapphire requires specialised techniques and is less established. The other potential substrate is silicon, which is widely used to study bactericidal mechanisms of nanotopographies. It can provide a flat surface enabling precise topographical control, but it

has fundamental limitations for medical device applications due to its low strength and fracture toughness. In our preliminary studies, after vitrification, Si substrates showed bubbling on the surface, making them unsuitable for further studies. On the other hand, titanium and its alloys (Ti-6Al-4V) represent the gold standard for orthopaedic and dental implants due to its superior biocompatibility, corrosion resistance, favourable mechanical properties and the nanopillar substrates are well characterised for their bactericidal action[2]. However, the primary disadvantage of titanium for cryo-EM workflows is its relatively lower thermal conductivity (21.9 W/m.K) compared to sapphire. Our substrate selection strategy prioritised clinical relevance over established cryo-optimised substrates, representing a broader trend in cryo-microscopy as the field expands beyond traditional cell biology applications into materials science and bioengineering. While sapphire remains optimal for fundamental cell biology studies where substrate material is irrelevant, emerging applications in biomaterials-cell characterisation increasingly requires the study of cells on clinically relevant substrates, despite their non-ideal cryo properties.

While our previous nanopillar fabrication work utilised bulk titanium substrates of 1 mm thickness and 1 cm in diameter, the current correlative cryo-microscopy workflow required adaptation to thin substrates for two critical reasons: 1) Thermal considerations – The high thermal mass and heat capacity of bulk titanium impede the rapid cooling rates required ($>10^4$ K/s) for successful vitrification. Thick metal substrates can act as heat sinks, promoting cubic ice crystal formation rather than vitreous ice, which introduces artefacts during vitrification; 2) Compatibility with cryo storage and transfers - Cryo-workflows require standardised sample dimensions to accommodate specialised transfer systems, storage containers, and sample holders across multiple instruments. Most commercial cryo-handling systems, including the Leica EM VCM, Leica EM VCT500 and associated stage holders are optimized for 3 mm diameter planchets, matching the standard TEM grid format (3.05 mm diameter copper grids). This standardisation enabled use of commercially available cryo-storage boxes and handling tools and easy transfer between modalities without need of custom adaptors.

Our workflow demonstrates that with appropriate sample geometry modifications and advanced vitrification methods, it is possible to achieve adequate ice quality on materials like titanium.

Vitrification Method Comparison

Rapid freezing of biological specimens can transform water into vitreous (amorphous) ice, effectively halting molecular motion and preserving cellular and macromolecular structures in a near-native state. This technique enables structural conservation of samples such as protein solutions, viruses, bacteria, and eukaryotic cells for EM, enabling structural analysis at resolutions approaching the atomic scale.[19] To prevent the formation of crystalline ice, cryo-fixation must achieve extremely rapid cooling rates, typically exceeding 100,000 °C per second. Importantly, vitrified samples are stable under the high-vacuum conditions used in cryo-EM and are also compatible with cryogenic fluorescence light microscopy (cryo-fLM).[2] While vitrification is well established for suspensions or adherent cells on EM grids, our study introduced a challenge to directly vitrify bacterial cells interacting with titanium substrate. Titanium poses unique challenges due to its lower thermal conductivity relative to Cu and sapphire disks, size, surface topography, and optical reflectivity, which complicate both freezing efficiency and correlative imaging. This work represents a key step towards enabling high-resolution structural analyses of bacteria–material interactions under fully hydrated, near-native conditions, bridging the gap between cryo-EM and material-biointerface science.

We have tested both plunge freezing and HPF in this workflow. Some of the plunge frozen samples showed ice crystal formation due to poor blotting, which were discarded. All plunge frozen samples had a crack on ice where they were held during the plunge freezing. All samples

also required clipping to an autogrid specimen cartridge to prevent damage and flake-off during the multiple handling steps required in the workflow, so that the sample could be held by the cartridge instead of the sample itself. It is important to note that some clipped samples popped out while handling in liquid nitrogen, as the c-clip could not hold the titanium substrate well enough in the cartridges. Once this occurred, they were hard to remount. These c-clips are designed to carry much thinner Cu TEM grids, which are 15-25 µm in thickness; hence, this is not a very favourable setup. Without cartridges, the plunge frozen samples were difficult to manipulate in the workflow. If thinner titanium foils were used, this popping out could have been avoided. However, we managed to locate bacteria and extract the lamella from a plunge frozen sample but at the final stage, during TEM tomography acquisition, the lamella was lost during transfer to the TEM, hence we could not acquire the cryo-tomogram from a plunge frozen sample.

With the HPF approach, a vitreous, reasonably flat substrate was achieved. The vitreous ice layer was thicker than for the plunge-frozen sample, so more material had to be removed and time taken to reach the titanium substrate during the FIB milling step. Given the large interaction volume and no blotting involved, vitrification was reproducible. Although we preferred HPF for our application, either of the techniques would work for sample vitrification in this workflow.

Hardware considerations in cryo-correlative tomography workflow

The successful implementation of our cryo-tomography workflow required careful consideration of hardware capabilities to ensure sample integrity and compatibility across modalities from different manufacturers **at geographically separated facilities** (IMG and TESCAN). Maintaining the vitreous state throughout all steps—from vitrification, fluorescence imaging, FIB milling and cryo-TEM imaging—demands a dedicated infrastructure capable of sustaining cryogenic temperatures and minimising exposure to humidity. Operating across equipment from multiple manufacturers (Leica transfer systems, TESCAN plasma FIB, JEOL TEM) introduced coordination challenges, making the standardised 3 mm sample format essential for cross-system compatibility. These hardware configurations were not incidental but **foundational to the workflow**, enabling high-resolution structural preservation and correlative targeting across imaging modalities at two geographically separated facilities. Our workflow demonstrates that advanced correlative cryo-microscopy is achievable without requiring all instrumentation to be co-located or from a single vendor.
Temperature control is critical throughout sample manipulation, otherwise the sample will go through thermal cycles where vitreous ice will crystallise. Therefore, the sample must be maintained below -135 °C (where initial recrystallisation starts to occur) at all times. The nanomanipulator must remain below −145 °C to preserve the vitreous state during lamella handling, while the sample stage must maintain <-145°C throughout FIB/SEM procedures. Our workflow utilised Leica VCM and VCT500 transfer systems, maintaining samples at ≤-180°C during exchange of samples between the instruments. Additionally, a humidity below 50% is essential to prevent ice contamination, which we were unable to achieve.

Cryo-compatible coating capabilities were essential for depositing conductive and protective layers without exposing samples to temperature rises or contamination. The system (Leica cryo-coater integrated with VCT500) enabled platinum or gold-palladium coating to minimize charging artefacts during imaging. Prior to FIB trench milling, an **organometallic platinum layer was deposited onto the cryo-sample surface using the Gas Injection System (GIS)** to provide a **protective cap** against **ion-beam damage and curtaining artefacts**. During the **cryo-lift-out**, however, **no GIS deposition was applied for lamella-to-grid attachment**, as in contrast to room-temperature workflows, **the lamella welding in cryogenic conditions was achieved through redeposition from the sample material itself.**

Fiducial-Based Fluorescence Correlation for Multi-facility Fluorescence Guided Targeting of Cryo-Lift-out Workflows

The challenge: Localising Bacteria on Vitrified Titanium substrates. One aim of this workflow was to assess the capacity of targeting a specific bacterium of interest to be studied, rather than picking a random bacterium in the presence of densely packed bacterial cells. However, localising and extracting a specific bacterium attached to a titanium nanopillar surface posed significant challenges during lamella preparation for cryo-electron tomography (cryo-ET). Bacterial cells attached to titanium nanopillars were buried 5-25 µm beneath the vitrified ice surface, making them invisible in cryo-SEM imaging. Hence, not just X-Y coordinates but also the Z depth was important. This is where correlative cryo-fluorescence microscopy was adapted as a complementary modality to identify buried bacteria. Once bound to SYTO9, bacterial DNA fluoresced green, indicating the location of the bacteria that otherwise could not be determined by cryo-SEM alone. Here we use a single stained bacterium as a proof-of-concept as to how cryo-fluorescence can guide subsequent electron imaging to improve the efficiency and precision of downstream cryo-EM or cryo-ET workflows. This can be expanded with other staining methods to identify specific bacteria of relevance to a study. However, while X-Y coordination was relatively successful, picking Z-direction was not always successful as we could not see the bacterial cell envelope directly interacting with the nanopillars. One reason could be that with fluorescence widefield imaging we picked a bacterium very close to the surface, yet 100-200 nm could not be resolved by widefield microscopy due to the surface topography, as seen in Figure 1a. Another reason could be that the tomography analysis was confined to a small region of the entire bacterium (200 nm), and another section of the bacterium could have been attached to the surface. However, gaps between nanopillars and the bacterial cell wall at the interface have already been reported in the literature, and can only be studied with a volume EM approach.

To overcome limitations related to finding a specific bacterium on the samples, we 1) adapted a surface feature-based correlation strategy and 2) developed a fiducial marker-based-correlation strategy that enabled reliable localisation of bacterial targets with high spatial precision. While both approaches were similar in concept, where a surface feature is correlated to the brightfield and SEM data, the surface feature-based strategy could be used for immediate lamella preparation using Ga-FIB, whereas the fiducial-marker strategy was needed for the combined FIB strategy, where no fluorescence facility was available. For the latter, bacterial cells were preselected, positions were marked on the surface and no image registration was required at the second facility. The key aspect was to create permanent FIB-milled fiducial patterns that were 1) cross-modality visible i.e. detectable by light microscope and electron microscopy; 2) permanent and ice contamination resistant i.e. milled features survived cryogenic storage, transport, and moderate ice contamination; 3) geometry defined - square pattern geometry enabled accurate coordinate transformation and easy image registration; and 4) reproducible i.e. the standardised pattern could be replicated across samples and laboratories easily.

These fiducials, milled into the sample surface prior to fluorescence imaging (Fig. 3), enabled reliable correlation between fluorescence data and FIB/SEM images across facilities, helping to preserve spatial accuracy throughout the workflow, despite the lack of integrated instrumentation. However, it is important to note that fiducials are visible in reflectance images and in SEM, but not in the fluorescence channel. As data is collected via two different channels of the light microscope, a slight misalignment of fluorescence and brightfield channels can lead to loss of the precise location and thus no tomogram at the end of the thinning and polishing, which is a major drawback.

Despite the isolation of a single bacterium within a 10 µm slab, a critical limitation arises after the initial 10 µm-thick slab is thinned for cryotomography due to over-milling. Without integrated fluorescence guidance, the location of the bacterium cannot be re-verified during thinning of the lamella. An additional step to check fluorescence would be helpful before thinning has started. During the thinning process, re-checking the sample in a cryo-fluorescence microscope would certainly help, but additional unloading and loading would increase the overall workflow time and the risk of ice contamination, potentially leading to total sample loss during manual handling. Consequently, we relied on getting the initial targeting right by keeping the bacterium at the centre while marking our fiducials when correlating fluorescence and SEM data sets. Even with careful alignment, there was still 500-1000 nm of uncertainty from the offset between reflected light and fluorescence channels. Despite this, we managed to capture surface-associated bacteria in 2 out of 4 attempts, which we consider reasonable given all the complications and limited availability of resources.

Limitations and opportunities of recent instrument developments. Recent studies have demonstrated the power of integrated cryo-FM-FIB-SEM systems in targeting fluorescently labelled organelles.[20] However, these systems are not widely available and were not accessible in our workflow. Our approach relied on stand-alone equipment, at two separate facilities: cryo-fluorescence imaging and initial Ga-FIB/SEM fiducial marking at IMG, and plasma cryo-FIB/SEM lamella preparation at TESCAN Factory, and TEM tomography back in IMG. This multi-facility correlative workflow introduced additional challenges beyond those of integrated systems: 1) Physical separation, where samples required cryogenic transport between facilities via dry shipper; 2) No real-time feedback - fluorescence correlation had to be established before plasma FIB milling, with no opportunity to re-check during the processing; 3) Ice contamination risk - multiple transfers increased frost accumulation on the sample surface; and 4) Coordinate preservation - bacterial positions identified by fluorescence had to be reliably relocated after transport and instrument changes.

Preparing electron-transparent cross-sections of bacteria attached to titanium nanopillar substrates presented unique challenges due to the disparate physical properties of biological and metallic materials. Bacteria and titanium differ significantly in both mechanical hardness during sectioning and thermal properties during vitrification, complicating sample preparation for correlative cryo-microscopy.

An additional bottleneck in the workflow was the reliability of cryo-lift-out and transfer steps; in some cases, lamellae were lost due to poor attachment to the cryo-nanomanipulator or insufficient adhesion to the TEM grid. Once they were deattached, recovering them was a tedious task and mostly ended in failure in our experience. This underscores the need for improved attachment strategies in cryo-conditions and robust cryo-transfer tools to enhance reproducibility in the future. During the lift-out procedure, especially when working with poorly conductive vitrified samples or insulating substrates, **electrostatic build up can cause the extracted lamella to shift or be lost entirely**, particularly in the final stages of transfer. This problem is exacerbated by the delicate nature of cryogenic conditions, where mechanical forces must be minimized and material grounding is often suboptimal. A critical bottleneck in non-integrated workflows occurs after slab extraction and placement onto a TEM grid for thinning. By using a copper block adaptor on the nanomanipulator needle enhances redeposition efficiency and stabilises lamella attachment during welding, reducing detachment risk during transfer.[21] Without integrated fluorescence imaging on the plasma FIB system, the precise location of the bacterium can no longer be tracked visually, and thinning often results in over-milling and loss of the target. While re-checking the grid in a cryo-fluorescence microscope

could potentially help, inter-system transfers increase the risk of ice contamination, require excessive time for transfer and can lead to further sample degradation through thermal cycling. These limitations underscore the value of pre-marking lamella positions using fiducial markers.

Future directions and workflow optimisation

While the current workflow demonstrates that reliable sample preservation and spatial targeting are feasible for characterising bacteria–material interactions in their native state, several instrument enhancements could significantly improve efficiency, throughput, and lamella yield. Sample preparation can be improved by adding cryo-protectant during the vitrification step. We have not used it as we wanted to characterise the interface as close as possible to native state. Adopting cryo protection will certainly improve the vitrification.

A key limitation remains the time-intensive nature of gallium-based FIB milling, which constrains the number of lamellae that can be prepared in a single session. In contrast, plasma FIB/SEM systems—such as those using xenon ion sources—offer substantially higher milling rates, enabling faster trenching and bulk material removal. This is especially advantageous when processing thick vitrified samples on metallic substrates like titanium, where milling depth and area are considerable. Xenon ions were particularly effective during the initial bulk-milling stage, where large volumes of hard material had to be removed under cryogenic conditions. Compared to gallium, Xe ions enabled milling at higher currents with improved beam profiles and reduced material redeposition, producing cleaner trenches and smoother cross-sections. As a result, the overall process yielded substantially faster and more reliable lamella preparation for subsequent cryo-lift-out. It is important to notice, at room temperature, milling of titanium with Ga beam at 30 kV is more efficient compared to plasma FIB.[22, 23] However, the redeposition we have noticed made the overall workflow less efficient in Ga at cryo temperatures. However, care must be taken to minimize potential artefacts associated with plasma beams, especially during final lamella polishing, as increased surface roughness or curtaining may occur at low polishing currents, which could compromise downstream cryo-TEM imaging. In our workflow, this was mitigated by performing the final polishing step on a separate Ga-based FIB system, which—owing to its narrower beam profile at low currents—enabled gentler and more controlled fine polishing with minimal curtaining. Although a hybrid approach combining Xe and Ga FIB systems was employed in this study, future applications of the methodology should not be limited by this setup, as the entire workflow can be implemented on a single instrument, provided the operator is aware of the respective strengths and limitations of each ion source.

To extend milling capacity, integration of an automated cryo-stage with active cooling would allow continuous 24-hour operation without requiring daily sample unloading, thus increasing throughput for lift-out-based lamella preparation. Furthermore, incorporating a cryo-fluorescence microscope directly within the FIB/SEM chamber would eliminate intermediate sample transfers between imaging modalities. This would reduce the risk of ice contamination and improve registration accuracy between fluorescence and electron imaging, which is critical for targeting 200 nm-thick lamellae for cryo-ET. Together, these technological improvements would streamline the correlative cryo-tomography workflow, enhancing reproducibility and enabling higher-throughput structural studies of microbial interactions at complex material interfaces.

Alternative Approaches and Future Developments — Several complementary strategies could further improve targeting precision: 1) Fluorescent fiducials on samples - addition of fluorescent beads or quantum dots directly to the sample before vitrification could serve as optical landmarks visible in both fluorescence and electron microscopy. However, this approach

requires careful design as fiducials must be spectrally distinct from bacterial fluorophores, their size and shape must be different from bacterial cells to avoid confusion when targeting, and brightness must be balanced, as they can obscure the fluorescence signal from bacteria when located in close proximity. Therefore, fiducial placement, intensity and spectral characteristics must be optimised to enhance registration accuracy without compromising visibility of the biological target.

In the meantime, fiducial-based surface marking, as demonstrated in our study (Fig. 1), remains a practical and robust solution to reduce localisation uncertainty and increase the success rate of cryo-lift-out and lamella preparation workflows for targeted bacterial tomography on biomimetic surfaces.

This strategy is generalisable beyond bacteria-nanopillar systems to any cryo-correlative workflow involving: 1) Non-transparent or optically challenging substrates (metals, ceramics, silicon, opaque polymers); 2) Multi-facility imaging pipelines requiring cryogenic sample transport between institutions 3) Targets embedded deep within vitrified ice (>5 µm from surface) where direct SEM visualization is impossible; 4) Systems where traditional EM grid landmarks are absent (custom substrates, medical device materials); 5) Serial lift-out workflows where multiple lamellae must be extracted from a single marked region.

For laboratories without access to integrated cryo-FM-FIB-SEM systems—which represents the majority of cryo-ET facilities globally—this approach is an affordable fluorescence-guided targeting without requiring expensive instrument upgrades.

Future improvements, such as integrated real-time fluorescence imaging, cryo-compatible super-resolution methods, and automated image correlation software, would further enhance the precision and efficiency of cryo-lamella workflows. Until such systems become widely available, physical fiducial markers remain an accessible and effective solution to bridge the gap between cryo-fluorescence imaging and high-resolution electron tomography.

Acknowledgements

This work was supported by the Engineering and Physical Sciences Research Council under UKRI Postdoc Guarantee (grant number EP/X022609/1). Access to cryo FIB/SEM and cryo TEM was supported by Czech-BioImaging project (Ministry of Education, project number LM2023050 Czech-BioImaging) at Electron Microscopy Core Facility, IMG ASCR, Prague, Czech Republic, which is supported by MEYS CR (LM2023050 Czech-BioImaging), OP RDE (CZ.02.1.01/0.0/0.0/18_046/0016045, CZ.02.1.01/0.0/0.0/16_013/0001775) and IMG grant (RVO: 68378050). The authors gratefully acknowledge the Wolfson Bioimaging Facility and the University of Bristol Workshop for their support and assistance in this work. Authors also acknowledge the Diamond Light Source (UK) Ltd for access to Helios Hydra via the experiment number BI35964, and the support by Dr. Dave Farmer and . C.D.B is currently funded by a Helmholtz recruiting initiative grant (I-044-16-01) awarded to Liane G. Benning from the GFZ. The authors thank Ufuk Borucu at University of Bristol, Dr. Benji Bateman and the mechanical workshop of Central Laser Facility of UKRI Science and Technology Facilities Council, and Samuel Zachej of Tescan Group a.s for their support. The authors thank group members of Oral Microbiology and bioMEG for their support and discussions.

Author Information and Contributions

Chaturanga D. Bandara; https://orcid.org/0000-0002-0688-4260

Dominik Pinkas https://orcid.org/0000-0002-6103-4314

Martina Zanova; https://orcid.org/0000-0002-6347-6167

Martin Uher; https://orcid.org/0009-0009-2646-1765

Judith Mantel; https://orcid.org/0000-0002-9061-8933

Bo Su; https://orcid.org/0000-0003-1063-8182

Angela H. Nobbs; https://orcid.org/0000-0003-3813-4410

Paul Verkade; https://orcid.org/ 0000-0002-2497-1026

References

(1) Baulin, V. A.; Linklater, D. P.; Juodkazis, S.; Ivanova, E. P. Exploring Broad-Spectrum Antimicrobial Nanotopographies: Implications for Bactericidal, Antifungal, and Virucidal Surface Design. *ACS Nano* **2025**, *19* (13), 12606-12625. DOI: 10.1021/acsnano.4c15671.
(2) Bhadra, C. M.; Khanh Truong, V.; Pham, V. T. H.; Al Kobaisi, M.; Seniutinas, G.; Wang, J. Y.; Juodkazis, S.; Crawford, R. J.; Ivanova, E. P. Antibacterial titanium nano-patterned arrays inspired by dragonfly wings. *Scientific Reports* **2015**, *5*, 16817, Article. DOI: http://dx.doi.org/10.1038/srep16817.
(3) Elbourne, A.; Crawford, R. J.; Ivanova, E. P. Nano-structured antimicrobial surfaces: From nature to synthetic analogues. *J Colloid Interface Sci* **2017**, *508*, 603-616. DOI: 10.1016/j.jcis.2017.07.021.
(4) Hasan, J.; Crawford, R. J.; Ivanova, E. P. Antibacterial surfaces: the quest for a new generation of biomaterials. *Trends Biotechnol* **2013**, *31* (5), 295-304. DOI: 10.1016/j.tibtech.2013.01.017.
(5) Bandara, C. D.; Singh, S.; Afara, I. O.; Tesfamichael, T.; Wolff, A.; Ostrikov, K.; Oloyede, A. Bactericidal Effects of Natural Nanotopography of Dragonfly Wing on Escherichia coli. *ACS Applied Materials & Interfaces* **2017**, *9* (8), 6746-6760. DOI: 10.1021/acsami.6b13666.
(6) Bandara, C. D.; Ballerin, G.; Leppänen, M.; Tesfamichael, T.; Ostrikov, K.; Whitchurch, C. B. Resolving Bio-Nano Interactions of E.coli Bacteria-Dragonfly Wing Interface with Helium Ion and 3D-Structured Illumination Microscopy to Understand Bacterial Death on Nanotopography. *ACS Biomaterials Science & Engineering* **2020**, *6* (7), 3925-3932. DOI: 10.1021/acsbiomaterials.9b01973.
(7) Jenkins, J.; Ishak, M. I.; Eales, M.; Gholinia, A.; Kulkarni, S.; Keller, T. F.; May, P. W.; Nobbs, A. H.; Su, B. Resolving physical interactions between bacteria and nanotopographies with focused ion beam scanning electron microscopy. *iScience* **2021**, *24* (7), 102818. DOI: 10.1016/j.isci.2021.102818.
(8) Imihami Mudiyanselage, C. C. D. B. Characterisation of the bactericidal efficacy of natural nano-topography using dragonfly wing as a model. PhD, 2017. https://eprints.qut.edu.au/106746/.
(9) Alameda, M. T.; Osorio, M. R.; Pedraz, P.; Rodríguez, I. Mechano-Dynamic Analysis of the Bactericidal Activity of Bioinspired Moth-Eye Nanopatterned Surfaces. *Advanced Materials Interfaces n/a* (n/a), 2200608. DOI: https://doi.org/10.1002/admi.202200608.
(10) Schiøtz, O. H.; Klumpe, S.; Plitzko, J. M.; Kaiser, C. J. O. Cryo-electron tomography: en route to the molecular anatomy of organisms and tissues. *Biochemical Society Transactions* **2024**, *52* (6), 2415-2425. DOI: 10.1042/bst20240173 (accessed 10/27/2025).
(11) Rice, W. J.; Cheng, A.; Noble, A. J.; Eng, E. T.; Kim, L. Y.; Carragher, B.; Potter, C. S. Routine determination of ice thickness for cryo-EM grids. *Journal of Structural Biology* **2018**, *204* (1), 38-44. DOI: https://doi.org/10.1016/j.jsb.2018.06.007.
(12) Jenkins, J.; Mantell, J.; Neal, C.; Gholinia, A.; Verkade, P.; Nobbs, A. H.; Su, B. Antibacterial effects of nanopillar surfaces are mediated by cell impedance, penetration and induction of

oxidative stress. *Nature Communications* **2020**, *11* (1), 1626. DOI: 10.1038/s41467-020-15471-x.
(13) Zachs, T.; Schertel, A.; Medeiros, J.; Weiss, G. L.; Hugener, J.; Matos, J.; Pilhofer, M. Fully automated, sequential focused ion beam milling for cryo-electron tomography. *eLife* **2020**, *9*, e52286. DOI: 10.7554/eLife.52286.
(14) Mastronarde, D. N. Automated electron microscope tomography using robust prediction of specimen movements. *J Struct Biol* **2005**, *152* (1), 36-51. DOI: 10.1016/j.jsb.2005.07.007 From NLM Medline.
(15) Hagen, W. J. H.; Wan, W.; Briggs, J. A. G. Implementation of a cryo-electron tomography tilt-scheme optimized for high resolution subtomogram averaging. *Journal of structural biology* **2017**, *197* (2), 191-198. DOI: 10.1016/j.jsb.2016.06.007 From NLM Medline.
(16) Reipert, S.; Fischer, I.; Wiche, G. High-pressure freezing of epithelial cells on sapphire coverslips. *Journal of Microscopy* **2004**, *213* (1), 81-85. DOI: https://doi.org/10.1111/j.1365-2818.2004.01260.x.
(17) McDonald, K.; Schwarz, H.; Müller-Reichert, T.; Webb, R.; Buser, C.; Morphew, M. Chapter 28 - "Tips and Tricks" for High-Pressure Freezing of Model Systems. In *Methods in Cell Biology*, Müller-Reichert, T. Ed.; Vol. 96; Academic Press, 2010; pp 671-693.
(18) Studer, D.; Humbel, B. M.; Chiquet, M. Electron microscopy of high pressure frozen samples: bridging the gap between cellular ultrastructure and atomic resolution. *Histochemistry and Cell Biology* **2008**, *130* (5), 877-889. DOI: 10.1007/s00418-008-0500-1.
(19) Matias, V. R. F.; Al-Amoudi, A.; Dubochet, J.; Beveridge, T. J. Cryo-Transmission Electron Microscopy of Frozen-Hydrated Sections of Escherichia coli and Pseudomonas aeruginosa. *Journal of Bacteriology* **2003**, *185* (20), 6112-6118. DOI: 10.1128/jb.185.20.6112-6118.2003.
(20) Yang, J.; Vrbovská, V.; Franke, T.; Sibert, B.; Larson, M.; Hall, A.; Rigort, A.; Mitchels, J.; Wright, E. R. Integrated Fluorescence Microscopy (iFLM) for Cryo-FIB-milling and In-situ Cryo-ET. *bioRxiv* **2023**, 2023.2007.2011.548578. DOI: 10.1101/2023.07.11.548578.
(21) Schiøtz, H. O.; Kaiser, O. J. C.; Klumpe, S.; Morado, R. D.; Poege, M.; Schneider, J.; Beck, F.; Klebl, P. D.; Thompson, C.; Plitzko, M. J. Serial Lift-Out: sampling the molecular anatomy of whole organisms. *Nature Methods* **2023**. DOI: 10.1038/s41592-023-02113-5.
(22) Brogden, V.; Johnson, C.; Rue, C.; Graham, J.; Langworthy, K.; Golledge, S.; McMorran, B. Material Sputtering with a Multi-Ion Species Plasma Focused Ion Beam. *Advances in Materials Science and Engineering* **2021**, *2021* (1), 8842777. DOI: https://doi.org/10.1155/2021/8842777.
(23) Burnett, T. L.; Kelley, R.; Winiarski, B.; Contreras, L.; Daly, M.; Gholinia, A.; Burke, M. G.; Withers, P. J. Large volume serial section tomography by Xe Plasma FIB dual beam microscopy. *Ultramicroscopy* **2016**, *161*, 119-129. DOI: 10.1016/j.ultramic.2015.11.001 From NLM.